Co-crystallization and Characterization of the Photosynthetic Reaction Center−Cytochrome c_2 Complex from *Rhodobacter sphaeroides*†

N. Adir,‡ H. L. Axelrod, P. Beroza,§ R. A. Isaacson, S. H. Rongey, M. Y. Okamura, and G. Feher*

Department of Physics 0319, University of California, San Diego, 9500 Gilman Drive, La Jolla, California 92093-0319

Received September 14, 1995; Revised Manuscript Received November 22, 1995⊗

ABSTRACT: The photosynthetic reaction center (RC) of *Rhodobacter sphaeroides* and cytochrome c_2 (cyt c_2), its physiological secondary electron donor, have been co-crystallized. The molar ratio of RC/cyt c_2 was found by SDS−PAGE and optical absorbance changes in the co-crystals to be 4. The crystals diffracted X-rays to 3.5 Å. However, the resolution degraded during data collection. A data set, 82.5% complete, was collected to 4.5 Å. The crystals belong to the tetragonal space group $P4_32_12$, with unit cell dimensions of $a = b = 142.7$ Å and $c = 254.8$ Å. The positions of the RCs in the unit cell were determined by molecular replacement. A comparable search for the cyt c_2 by this method was unsuccessful because of the small contribution of the cytochrome to the total scattering and because of its low occupancy. The cyt c_2 was positioned manually into patches of difference electron density, adjacent to the periplasmic surface of the M polypeptide subunit of the RC. The difference electron density was not sufficient for precise positioning of the cyt c_2, and its orientation was modeled by placing the exposed edge of the heme toward the primary donor of the reaction center D and by forming pairs for electrostatically interacting RC and cyt c_2 amino acid residues. The RC−cyt c_2 structure derived from the co-crystal data was supported by use of omit maps and structure refinement analyses. Cyt c_2 reduces the photooxidized primary donor D^+ in 0.9 ± 0.1 μs in the co-crystals, which is the same as the fast electron transfer rate *in vivo* and in solution. This result provides strong evidence that the structure of the complex in the co-crystal is the same as in solution. Two additional methods were used to investigate the structure of the RC−cyt c_2 complex: (i) Docking calculations based on interprotein electrostatic interactions identified possible binding positions of the cyt c_2 on the RC. The cyt c_2 position with the lowest electrostatic energy is very similar to that of the cyt c_2 in the proposed co-crystal structure. (ii) Site-directed mutagenesis was used to modify two aspartic acid residues (M184 and L155) on the periplasmic surface of the RC. Cyt c_2 binding affinity to these RCs and electron transfer rates to D^+ in these RCs support the co-crystal structure of the RC−cyt c_2 complex.

In photosynthesis, the primary photochemical reactions occur within a membrane-bound pigment−protein complex called the reaction center (RC).[1] RCs from the purple nonsulfur bacteria *Rhodopseudomonas viridis* and *Rhodobacter sphaeroides* have been extensively characterized by biophysical methods [for reviews, see Feher and Okamura (1978), Feher *et al*. (1989), Deisenhofer and Michel (1991), Gunner (1991), Breton and Vermeglio (1992), and Feher (1992)]. The three-dimensional structures of these RCs have been determined by X-ray crystallography (Deisenhofer *et al*., 1984, 1985; Allen & Feher, 1984; Chang *et al*., 1986, 1991; Allen *et al*., 1986, 1987a,b, 1988; Yeates *et al*., 1987; El-Kabbani *et al*., 1991; Chirino *et al*., 1994; Ermler *et al*., 1994; Arnoux *et al*., 1995) and serve as models for other photosynthetic complexes and membrane proteins (Michel & Deisenhofer, 1988; Rees *et al*., 1989).

The RCs of *Rps. viridis* and *Rb. sphaeroides* are structurally homologous and perform similar photochemical reactions. The RCs from both species contain a membrane-bound polypeptide core, composed of three subunits called L, M, and H (Feher & Okamura, 1978; Feher *et al*., 1989; Deisenhofer & Michel, 1991), which bind eight cofactor molecules and one non-heme iron. Upon illumination, the primary donor D, a bacteriochlorophyll dimer, is excited and an electron is transferred consecutively to three electron acceptors: a bacteriopheophytin and two ubiquinone molecules, Q_A and Q_B. A major difference between RCs from *Rps. viridis* and *Rb. sphaeroides* is the secondary electron donor that reduces the photooxidized primary donor, D^+. In *Rps. viridis*, a tetra-heme *c*-type cytochrome is tightly bound to the membrane polypeptide core of the RC. Its three-dimensional structure was determined as an integral part of the RC (Deisenhofer & Michel, 1991; Deisenhofer *et al*.,

† Work supported by the National Science Foundation (NSF MCB93-04782), National Institutes of Health (NIH GM 13191), and U.S. Department of Agriculture (USDA 93-37306-9579 and 93-37306-9182).

* To whom correspondence should be addressed.

‡ Present address: Department of Chemistry, Technion, Technion City, Haifa 32000, Israel.

§ Present address: Scripps Research Institute, MB1, 10666 N. Torrey Pines, La Jolla, CA 92037.

⊗ Abstract published in *Advance ACS Abstracts*, February 1, 1996.

[1] Abbreviations: AML, artificial mother liquor; RC, reaction center; $[RC]_{total}$, and $[RC]_{free}$, concentrations of total and free reaction center; cyt c_2, cytochrome c_2; $[C]_{free}$, $[C]_{total}$, and [C·RC], concentrations of free, total, and cyt c_2 bound to RCs, respectively; D, primary donor in bacterial reaction centers; D^+, the photooxidized primary donor; DM, dodecyl β-D-maltoside; EDTA, ethylenediaminetetraacetic acid; HT, heptanetriol; K_D, RC−cyt c_2 dissociation constant; k_0, second-order electron transfer rate constant; LDAO, lauryldimethylamine oxide; PEG 4000, poly(ethylene glycol) molecular weight 4000; Q_0, ubiquinone without an isoprenoid chain; SDS−PAGE, sodium dodecyl sulfate−polyacrylamide gel electrophoresis; τ_e, first-order electron transfer time constant; TLE buffer, 10 mM Tris-HCl (pH = 8.0), 0.025% LDAO, and 1 mM EDTA.

0006-2960/96/0435-2535$12.00/0 © 1996 American Chemical Society

1984, 1985). In *Rb. sphaeroides*, the secondary electron donor to D^+ is a water-soluble single heme cytochrome c_2 (cyt c_2) [for reviews on cytochromes, see Bartsch (1978) and Moore and Petigrew (1990)], which reversibly binds to the RC. The three-dimensional structure of cyt c_2 from *Rb. sphaeroides* has recently been determined (Axelrod *et al*., 1994).

The cytochrome binding site in *Rps. viridis* is located on the periplasmic side of the RC core, directly above D, as determined from the X-ray crystal structure. Previous studies have shown that, in *Rb. sphaeroides*, a single cyt c_2 (Rosen *et al*., 1980) binds to the periplasmic side of the RC (Prince *et al*., 1975). The site is formed by hydrophilic stretches of the L and M polypeptides of the RC as shown by chemical cross-linking studies (Rosen *et al*., 1983). Evidence of the importance of electrostatic interactions in the docking of cyt c_2 to the RC of *Rb. sphaeroides* is provided by the following experimental findings: (i) The binding affinity of the RC−cyt c_2 complex decreases with increasing ionic strength, consistent with counterion screening of favorable electrostatic interactions of the docked structure (Moser & Dutton, 1988; Wachtveitl *et al*., 1993). The electrostatic complementarity in forming the docked complex arises from interactions between acidic residues of the RC with positive residues of the cyt c_2 (Okamura & Feher, 1983). (ii) Chemical modification of positively charged residues near the exposed heme edge of the cyt c_2 was shown to reduce the binding affinity between the proteins (Long *et al*., 1989). (iii) Mutation of aspartic acid residues on the periplasmic surface of the RC reduces the binding affinity of cyt c_2 (Rongey *et al*., 1994).

The reaction kinetics of the reduction of D^+ by cyt c_2 are biphasic [Overfield *et al*., 1979; see review by Mathis (1994)]. The fast phase ($\tau_e \sim 1$ μs) follows first-order kinetics and is due to electron transfer from cyt c_2 bound to the RC. The amplitude of the fast phase is thus proportional to the fraction of RCs that have a bound cyt c_2. The slow electron transfer phase follows second-order kinetics and is limited by the rate of encounter of a cyt c_2 with an RC. This encounter is a diffusive process that is accelerated by intermolecular electrostatic attraction.

Two models for the RC−cyt c_2 complex have been previously proposed. In the model of Allen *et al*. (1987) the cyt c_2 was manually docked to a position analogous to that of the *Rps. viridis* cytochrome, directly above D. Tiede and co-workers proposed a second model, based on linear dichroism measurements (Tiede, 1987), manual docking (Tiede *et al*., 1988), and electrostatic calculations (Tiede & Chang, 1988); in their model the binding site is shifted toward the M subunit side of the RC. In both models, the electrostatic interactions between negatively charged amino acids on the RCs periplasmic surface and positively charged amino acid residues surrounding the heme crevice of cyt c_2 are assumed to stabilize the bound complex. This assumption is supported by the effect of ionic strength on cyt c_2 binding as described above.

The most direct way to investigate the spatial interaction between the RC and cyt c_2 from *Rb. sphaeroides* is to determine the three-dimensional structure of the bound complex by X-ray diffraction analysis. This requires the co-crystallization of the complex. A similar approach has been used for the bimolecular complex of yeast cytochrome *c* peroxidase−iso-1-cytochrome *c* (Pelletier & Kraut, 1992) and the trimolecular complex amicyanine−methylamine dehydrogenase−cytochrome c_{551i} (Chen *et al*., 1993).

In the present work, we report on the co-crystallization of the RC−cyt c_2 complex from *Rb. sphaeroides*. An X-ray diffraction data set obtained from a co-crystal was used to construct a structural model of the RC−cyt c_2 complex. To establish whether the crystallized RC−cyt c_2 complex corresponds to the physiological complex, we compared the intermolecular electron transfer kinetics in the co-crystals with those in solution. Two additional approaches were used to provide supporting evidence for the proposed structure: (i) A computational search for possible binding sites, based on electrostatic interactions between the proteins, was made; the lowest energy docked structure was compared to the proposed RC−cyt c_2 structure. (ii) Two aspartic acid residues were mutated to lysines on the periplasmic side of the RC. From the effect of the mutations on the cyt c_2 binding affinity, the points of contact between the RC and cyt c_2 were deduced and compared to the proposed structure.

The results of the above experiments are used to compare the different models of the RC−cyt c_2 complex, and the relation between the proposed structure and electron transfer is discussed. The RC−cyt c_2 complex serves as a model to understand other electron transfer systems, in which mobile, hydrophilic proteins transport electrons between membrane-bound protein complexes. Preliminary accounts of this work have been presented (Rongey *et al*., 1994; Adir *et al*., 1994; Rongey, 1994).

EXPERIMENTAL PROCEDURES

Protein Purification and Characterization. RC and cyt c_2 were purified from *Rb. sphaeroides* as described (Feher & Okamura, 1978; Bartsch, 1978; Axelrod *et al*., 1994) with the following additions: the proteins were applied to a PL-SAX 1000 Å (Western Analytical) anion-exchange HPLC column (attached to a Beckman Gold HPLC System), equilibrated in 10 mM Tris-HCl (pH = 8.0), 1.0 mM EDTA, and 0.025% (w/v) LDAO (TLE buffer). The proteins were eluted with NaCl gradients (0−200 mM for RC and 0−100 mM for cyt c_2). The purity of the isolated RC and cyt c_2 was determined by the optical absorption ratio A_{280nm}/A_{802nm} ($\leq$1.2; Feher & Okamura, 1978) and A_{280nm}/A_{417nm} ($\leq$0.25; Bartsch, 1978), respectively. The purity was additionally confirmed by SDS−PAGE (Laemmli, 1970). The purified proteins were dialyzed against TLE buffer and concentrated with Centricon-30 ultrafiltrators (Amicon) to at least 35 mg/mL.

Crystallization. Co-crystallization of the RC and cyt c_2 was performed by vapor diffusion using sitting drops of the crystallization solution (McPherson, 1990) at 19 °C in Cryschem type plates (Charles Supper). Twenty microliter drops containing equimolar concentrations of 70 μM RC and cyt c_2 each (corresponding to a total protein concentration of 7.5 mg/mL), 10% (w/v) PEG 4000, 0.06% (w/v) LDAO, 4% (w/v) HT, 10 mM NaCl in 50 mM Tris-HCl (pH = 8.5), 0.1% (w/v) NaN_3, and 1 mM EDTA were equilibrated against at 1 mL reservoir solution, containing 22% (w/v) PEG 4000 and 0.3 M NaCl in 50 mM Tris-HCl (pH = 8.5). Manipulation of crystals was performed in the presence of added artificial mother liquor (AML; 20% PEG 4000, 50 mM Tris (pH = 8.5), 0.06% LDAO, 4% HT, 20 mM NaCl). For SDS−PAGE analysis, ~25 crystals per lane were

washed twice with AML, and the crystals were dissolved in 10 mM Tris-HCl (pH = 8.5) and 0.1% LDAO to prevent protein aggregation prior to solubilization of the proteins in SDS sample buffer. Analysis of the Coomassie brilliant blue stained gels was performed using a Bio-Rad GS-670 imaging densitometer.

Data Collection and Molecular Replacement. Data were collected from a single crystal at room temperature, using Cu Kα radiation from a RU-300 rotating anode X-ray generator and a Rigaku R-AXISIIc imaging plate area detector. Due to X-ray-induced degradation of the resolution from the initial 3.5 Å a data set was collected to 4.5 Å; it was 82.5% with 13503 unique reflections. The reflections were indexed and merged using the R-AXIS software package. The R_{merge} factor (defined as $R = \sum|I_i - I_j|/\sum|I_i + I_j|$, where the measured intensities I are summed over all symmetry-related reflections i and j) was 0.12. Analysis of the diffraction data showed the crystal to be tetragonal with unit cell dimensions of $a = b = 142.7$ Å and $c = 254.8$ Å. The space group was initially assigned as $P422$. Molecular replacement [reviewed in Rossman (1990)] was performed to determine the position of the RC in the co-crystal, using the integrated software package MERLOT version 2.3 (Fitzerald, 1988; Crowther, 1972). The refined molecular coordinates for the RC (entry P4RCR, Protein Data Bank, Brookhaven) were used as the search model, following rotation of the Euler angle β by 45° and translation of the origin of the coordinates to the RC center of mass as suggested in the MERLOT package (Fitzerald, 1988).

Calculation of Electrostatic Energies of Docked Structures. To investigate possible cyt c_2 docking positions on the RC periplasmic surface, we used the method of Roberts *et al*. (1991) to build a set of putative docked structures. This method systematically samples the relative orientations of the two proteins and generates a large set of docked structures from which a subset having the lowest electrostatic energy was identified. Following Roberts *et al*. (1991), docked RC−cyt c_2 structures were generated by the following procedure:

(1) Generation of Surfaces. For each atom, a set of points (density of ∼3 Å^{-2}) was generated on the van der Waals surface [atomic radii were taken from Yang *et al*. (1993)]. Points that penetrated van der Waals radii of other atoms were eliminated, thus defining a van der Waals surface for the two proteins.

(2) Identification of Docking Axis. For every pair of points on the van der Waals surfaces (one on the RC and one on the cyt c_2), the cyt c_2 was positioned such that the pair of points coincided and were collinear with the center of mass of both proteins. The docking axis was defined as the line that passes from the center of mass of the RC, through the point of contact of the van der Waals surfaces, to the center of mass of the cyt c_2.

(3) Rotation and Translation of the Cyt c_2. The cyt c_2 was rotated in 20° increments about the docking axis and translated along the axis to avoid steric overlap between the two proteins. Thus, 18 docked complexes were generated for each docking axis.

(4) Calculation of the Intermolecular Electrostatic Energy. The electrostatic interaction energy was calculated for each docked complex by Coulomb's law using a dielectric constant of 80.[2] Atomic charges were taken from the DISCOVER parameter set (Hagler *et al*., 1974); all lysine, arginine, glutamic acid, and aspartic acid residues were considered to be in their charged state.

The number of docked structures generated by this algorithm is $N = n_{RC}n_{cyt}n_\theta$, where N is the number of docked structures, n_{RC} and n_{cyt} are the number of surface points for the RC and cyt c_2, and n_θ is the number of angles sampled about the docking axis. There were ∼1200 surface points for the RC (only points on the periplasmic surface were considered), ∼2000 for the cytochrome, and 18 rotational angles searched about each docking axis, making a total of ∼10^7 docked structures. To improve the computational efficiency, the properties of the RC (volume and electrostatic potential) were mapped onto a cubic grid of 1 Å spacing. This permitted rapid determination of both the steric overlap and electrostatic interaction between the proteins because (i) the atomic coordinates for each cyt c_2 position could be quickly compared with nearby grid points to evaluate steric overlap and (ii) the electrostatic potential resulting from the RC charges needed to be calculated only once. The total interaction energy was obtained by multiplying the charge on each cyt c_2 atom by the electrostatic potential (generated by the RC charges) at the nearest grid point. The accuracy in the position of the cyt c_2 is limited by the 20° rotation steps for each docking axis examined and the discretization onto the grid of the calculated electrostatic potential of the RC surface due to the grid spacing. For the 1000 lowest energy docked structures identified by this procedure, a more accurate electrostatic interaction energy was obtained using the atomic coordinates (rather than the grid representation of the RC as used above). This provided a more accurate energy by avoiding discretization errors in the electrostatic potential associated with the grid used in the previous search.

Site-Directed Mutagenesis. The construction of site-directed mutant RCs was performed as described (Paddock *et al*., 1989, 1990), with a few modifications as noted. Two mutants, each with a single Asp → Lys change, were constructed; the codon for Asp (GAC) was changed to the codon for Lys (AAG). The Asp → Lys substitution was made at position L155 or M184, resulting in the DK(L155) or DK(M184) mutant, respectively. Each mutation was incorporated into a M13 vector containing the DNA coding for the L or M subunit (Rongey, 1994; Paddock *et al*., 1990). The sequence around each mutation showed no other changes in the subcloned regions. Each mutated DNA sequence was introduced into a pRK expression vector containing the upstream and downstream regions of the *puf* operon (Rongey, 1994; Paddock *et al*., 1989, 1990). Each mutant *puf* operon was transferred into the *Rb. sphaeroides* deletion strain ΔLM1 for the production of mutant RCs.

Measurements of Electron Transfer Kinetics. *(A) In Crystals*. A microspectrophotometer of local design (Allen & Feher, 1984) was modified to use a home-built flash unit for the measuring beam, and the output from the photomultiplier tube (Hamamatsu, R928) was connected directly to a digital LeCroy 9310M oscilloscope for data accumulation and signal averaging. Data were analyzed using com-

[2] This value is likely to be an overestimate. However, we are only interested in the relative energies of the different structures, the order of which is insensitive to the absolute value of the dielectric constant.

mercially available software (Sigmaplot, Peakfit; Jandel). A relatively large bandwidth (8 nm) was used for the measuring beam to improve the signal to noise ratios. The crystals were incubated in AML buffer with 1 mM terbutryn and mounted in 1.0 mm capillary tubes (Charles Supper); terbutryn replaces the secondary electron acceptor Q_B, the concentration of which is variable in crystallized RCs. For measurement of electron transfer from cyt c_2 to the RCs, 1 mM ascorbic acid was added to the incubation buffer; ascorbic acid ensures that cyt c_2 is reduced but does not reduce D^+ during the measurement.

Photooxidation of the RCs ($D \rightarrow D^+$) was achieved by directing the flash from a ruby laser ($\lambda = 695$ nm, ~30 ns pulse width) onto the crystal using a light guide. The resolution of the system was limited by the decay of the overshoot (~0.2 μs) caused by the scattered light from the sample following the laser flash. For signal averaging, excitation of the crystal was performed once every 10 min, which allowed the system to return to its original state (reduced cyt c_2 and oxidized Q_A).

(B) In Solution. The difference extinction coefficients $\Delta\epsilon^{\lambda}_{RC}$ ($DQ_A \rightarrow D^+Q_A^-$) and $\Delta\epsilon^{\lambda}_{cyt}$ (cyt $c_2^{2+} \rightarrow$ cyt c_2^{3+}) were determined for 502 and 545 nm using the microspectrophotometer. The coefficients for charge separation ($\Delta\epsilon^{\lambda}_{RC}$) were determined by photooxidizing an RC solution with a flash from the ruby laser. The coefficients for cyt c_2 oxidation ($\Delta\epsilon^{\lambda}_{cyt}$) were determined by chemically reducing (addition of ascorbic acid) and oxidizing (addition of ferricyanide) cyt c_2; for these measurements a continuous wave measuring beam was used, and the output of the photomultiplier was amplified (gain = 10).

The reaction of cyt c_2 with the RC in solution was monitored optically at 595 or 865 nm and recorded on a Cary 14 spectrophotometer (Varian). This system previously described (Kleinfeld *et al*., 1984) was modified in this work to obtain faster time resolution ($\tau \cong 70$ ns). For a monitoring wavelength of 595 nm, the ruby laser (see above) was used to excite the RCs. For a monitoring wavelength of 865 nm, either the ruby laser or a chemical dye laser (Phase-R, now Lumen-X) ($\lambda = 590$ nm, rhodamine 6G dye, pulse width ~0.4 μs) was used. Measurements were performed in 10 mM HEPES (pH = 7.5) with 0.04% (w/v) DM and 0.1 mM EDTA at 23 °C. Solutions of quinol and quinone were added to the sample to a concentration of 0.1 mM each prior to measurement to ensure reduction of the cyt c_2 and to allow signal averaging of multiple flashes.

The electron transfer reaction kinetics between cyt c_2 and the RC in solution proceeds in two phases as has been previously described [reviewed in Mathis (1994)]. From the fast phase the electron transfer time (τ_e) for the bound complex was obtained. The second-order rate constant (k_0) and the dissociation constant (K_D) were obtained from the absorption changes as a function of cyt c_2 concentration by the following procedure: The equilibrium concentration of the bound complex ([C·RC]) was determined from the portion of the absorption change associated with the fast-phase kinetics and the total RC concentration, $[RC]_{total}$. The concentration of free cyt c_2 was calculated by subtracting the portion of cyt c_2 that reacted with fast kinetics from the total cyt c_2 concentration ($[C]_{free} = [C]_{total} - [C\cdot RC]$). The concentration of free RC was calculated in a similar fashion. The dissociation constant, K_D, was determined by plotting the ratio of bound RC to free RC ($[C\cdot RC]/[RC]_{free}$) versus the free cyt c_2 concentration, $[C]_{free}$; the slope of this plot is $1/K_D$. The second-order rate constant (k_0) was determined by plotting the observed slow-phase rate constant (k_{obs}) versus the concentration of free cyt c_2 ($[C]_{free}$); the slope of this plot is k_0.

RESULTS

Characterization of the Crystallized RC−Cyt c_2 Complex. *(A) Crystal Parameters*. There are several inherent difficulties associated with the successful crystallization of the RC−cyt c_2 complex: (i) the RC is hydrophobic while the cyt c_2 is hydrophilic; (ii) formation of the RC−cyt c_2 complex is an equilibrium process, and thus the crystallization solution contains an inherent heterogeneity with fractions of free RC, free cyt c_2, and bound complex; and (iii) the two proteins have different solubility in the presence of precipitating agents necessary for crystallization [see Allen *et al*. (1987) and Axelrod *et al*. (1994) for precipitant concentrations of free RC and cyt c_2]. For these reasons, and because the RC is the major protein component, RC crystals with a needle form that contained no cyt c_2 were frequently observed [these crystals were found to be similar to the orthorhombic form described in Allen *et al*. (1986)]. Similar shaped crystals were also observed when cyt c_2 was absent from the crystallization mixture. When the crystallization parameters were modified to promote complex formation (low ionic strength) and to limit crystallization of the RCs alone (changes in the concentration of the precipitant and pH), crystals with a tetragonal pyramidal shape were formed. These crystals grew only in the presence of cyt c_2, usually within 3 weeks, to a maximum size of 0.3 mm × 0.3 mm × 0.1 mm. Analysis of the X-ray diffraction pattern showed the crystal to belong to the tetragonal space group *P*422 (Laue class *P*4/*mmm*) with unit cell dimensions of $a = b =$ 142.7 Å and $c = 254.8$ Å. Although systematic absences of some reflections were observed, they were not sufficiently conclusive to assign the crystal to one of the eight possible space groups. Consequently, the assignment was made on the basis of the molecular replacement solution as discussed in a later section.

(B) Cyt c_2−RC Stoichiometry in the Tetragonal Crystals. The average [RC]/[cyt c_2] ratio in the co-crystals was determined by SDS−PAGE (Figure 1). The co-crystals were thoroughly washed prior to solubilization to avoid nonspecifically associated cyt c_2 on the outside surface of the crystal. The gel shown in Figure 1 clearly shows the presence of cyt c_2 (lane 2), confirming that these are indeed co-crystals. The [RC]/[cyt c_2] molar ratio was determined by optical densitometry of the Coomassie brilliant blue stained gel (see insert in Figure 1), comparing solubilized crystals to solutions of known composition. The [RC]/[cyt c_2] ratio was determined to be 4.0 ± 0.5. Other crystal forms found in some crystallization trials had no identifiable cyt c_2 when analyzed in a similar fashion by SDS−PAGE. An alternative way to measure the [RC]/[cyt c_2] stoichiometry utilizing optical absorbance changes following a laser flash is discussed in the next section.

(C) Electron Transfer in the Co-crystal. The stoichiometry of the crystallized complex was also investigated by measuring interprotein electron transfer activity in the co-crystal, using the microspectrophotometer and laser excitation.

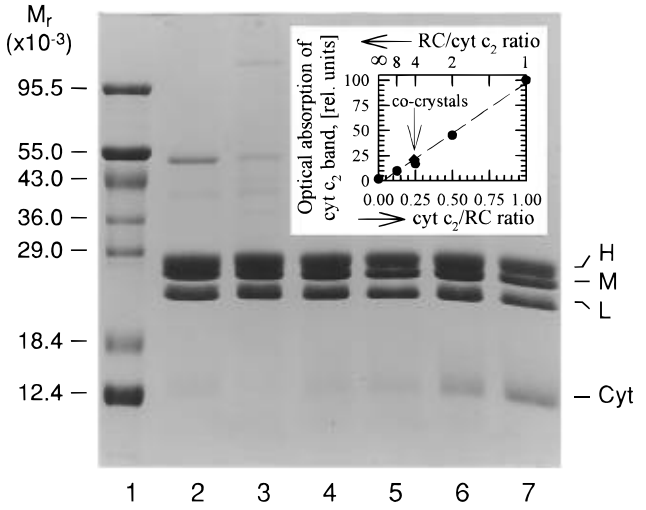

FIGURE 1: SDS−PAGE analyses of solubilized co-crystals. Co-crystals were washed twice in artificial mother liquor, pelleted, dried, and dissolved in 10 mM Tris (pH = 8.0) + 0.1% LDAO. The proteins were then solubilized in SDS−PAGE sample buffer and separated on a 10−13% gradient acrylamide gel. Lanes: 1, molecular weight standards; 2, solubilized co-crystals; 3−7, standard solution mixtures (12 μg of RC protein/lane) at different molar ratios of [RC]/[cyt c_2]: ∞ (lane 3), 8 (lane 4), 4 (lane 5), 2 (lane 6), and 1 (lane 7). The insert shows densitometric analysis of the stained cyt c_2 bands of the gel. The integrated density of the stained cyt c_2 band in each lane was normalized to the integrated densities of the stained RC bands. Symbols: closed circles, standard solutions; closed diamond, solubilized co-crystals. The ratio of RC/cyt c_2 in the co-crystal was determined to be 4.0 ± 0.5 by comparing the optical absorbance of the cyt c_2 band from the co-crystal with those from the standards.

Table 1: Extinction Coefficients (in mM^{-1} cm^{-1}) Associated with Electron Transfer in the RC−Cyt c_2 Complex[a]

	activity	
λ (nm)	charge separation $\Delta\epsilon_\lambda^{RC}$ (D → D$^+$)[b]	cyt c_2 oxidation Δ_λ^{cyt} (cyt c_2^{2+} → cyt c_2^{3+})[c]
502	5.9 ± 0.7	−0.1 ± 0.4
545	9.3 ± 1.1	−15.2 ± 0.4

[a] Extinction coefficients were determined using solutions of RCs or cyt c_2 in the microspectrophotometer. The measuring beam had a bandwidth of 8 nm, as used for co-crystal measurements. Thus, the $\Delta\epsilon$'s are effective extinction coefficients, valid for the microspectrophotometer; the real extinction coefficients are larger. [b] Charge separation for a RC solution was induced with a laser flash. [c] Cyt c_2 solutions (10 mM Tris, pH 8) were reduced (cyt c_2^{2+}) with 10 mM ascorbic acid or oxidized (cyt c_2^{3+}) with 10 mM potassium ferricyanide.

Following a laser excitation flash, the charge separated state $D^+Q_A^-$ is formed in all RCs. In the co-crystals, reduction of $D^+Q_A^-$ to DQ_A^- occurs only in those centers that contain reduced cyt c_2 (concomitantly resulting in the oxidation of cyt c_2^{2+} to cyt c_2^{3+}). In centers that lack cyt c_2, the state $D^+Q_A^-$ decays to DQ_A in about 0.1 s [reviewed in Feher *et al.* (1989)], which is much longer than the electron transfer rate from cyt c_2 to the RC. Absorption changes associated with D and the cyt c_2 heme were measured spectroscopically at 545 and 502 nm as described below.

The absorption changes due to charge separation and cyt c_2 oxidation at 545 and 502 nm are summarized in Table 1. To check the assumption that the extinction coefficients for charge separation are the same in crystals as in solution, measurements were performed using co-crystals containing oxidized[3] cyt c_2 (Figure 2a). In Figure 2a, the ratio of the absorption changes at 545 and 502 nm is 1.5 ± 0.1. This

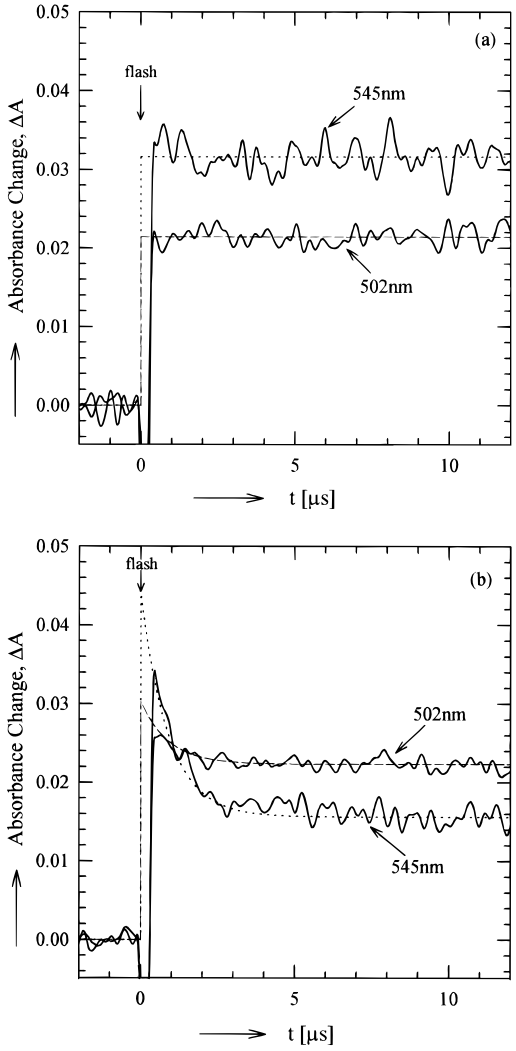

FIGURE 2: Light-induced absorption changes in co-crystals where cyt c_2 is (a) oxidized and (b) reduced; each trace is an average of nine flashes. Crystals were mounted in quartz capillary (1 mm) tubes, in artificial mother liquor with terbutryn (1 mM) in (a) and (b) and ascorbic acid in (b). The crystals were monitored at 545 and 502 nm with a bandwidth of 8 nm and excited by a ruby laser pulse (695 nm). The negative spike is an artifact due to scattering of the laser flash by the crystal. In the co-crystal with oxidized cyt c_2 (a) the absorption changes are due to photooxidation of the donor (D → D$^+$). In the co-crystal with reduced cyt c_2 (b) the absorption changes are the sum of the positive absorption change in RCs (D → D$^+$) and the negative change due to the concomitant reduction of D$^+$ and the oxidation of cyt c_2 in those RCs which bind cyt c_2 (D^+ + cyt c_2^{2+} → D + cyt c_2^{3+}). The values obtained from the measurements in (b) were used to calculate a RC/cyt c_2 ratio of 4.0 ± 0.3. This agrees with the value obtained from Figure 1. From a fit of the kinetics to the function $\exp(-t/\tau_e)$ a value of $\tau_e = 0.9 \pm 0.1$ μs was obtained. This value is, within experimental error, the same as obtained in solution.

ratio is the same, within experimental error, as the ratio of the extinction coefficients determined in solution ($\Delta\epsilon_{545}^{RC}/\Delta\epsilon_{502}^{RC} = 1.6 \pm 0.2$; see Table 1).

To determine the fraction of RCs that react with cyt c_2, and the time constant for this reaction, the co-crystals were incubated with ascorbic acid to reduce the cyt c_2 in the crystals. The results obtained on one of the co-crystals is

[3] During the time required for co-crystal formation (weeks) cyt c_2 becomes oxidized; addition of ferricyanide (1 mM), to ensure that cyt c_2 was oxidized, did not alter the ratio of the absorption changes at 545 and 502 nm.

shown in Figure 2b. Following the flash, the induced charge separation decays due to reduction of D^+ by cyt c_2 according to the scheme

$$DQ_A{\cdot}\text{cyt } c_2^{2+} + h\nu \rightarrow D^+Q_A^-{\cdot}\text{cyt } c_2^{2+} \xrightarrow{\tau_e} DQ_A^-{\cdot}\text{cyt } c_2^{3+} \quad (1)$$

where τ_e represents the characteristic time of electron transfer from cyt c_2^{2+} to D^+.

The optical absorption change, relative to the preflash value, as a function of time is given by

$$\Delta A_\lambda(t) = \Delta\epsilon_\lambda^{RC}([RC] - [\text{cyt } c_2^{3+}](t))l + \Delta\epsilon_\lambda^{cyt}[\text{cyt } c_2^{3+}](t)l \quad (2)$$

where the $\Delta\epsilon_\lambda$'s are the extinction coefficients summarized in Table 1, l is the optical path length, [RC] is the RC concentration in the co-crystal and [cyt c_2^{3+}](t) is the time-dependent concentration of cyt c_2^{3+} in the co-crystal.

The time dependence of the observed absorption decay was fitted with $\exp(-t/\tau_e)$ (dashed and dotted lines in Figure 2b), from which the value for the electron transfer time

$$\tau_e = 0.9 \pm 0.1\ \mu s \quad (3)$$

was determined. This time is, within experimental error, the same as obtained in solution. This provides strong evidence that the docked structures in the co-crystal and in solution are very similar.

At $t = 0$, the ratio of the amplitudes $\Delta A_{545}/\Delta A_{502} = \Delta\epsilon_{545}^{RC}/\Delta\epsilon_{502}^{RC}$, the same as for a co-crystal in which cyt c_2 is oxidized. The value obtained was 1.5 ± 0.1, which is in agreement with the value obtained from Figure 2a.

At $t \gg \tau_e$, the value of [cyt c_2^{3+}](t) equals the concentration of RCs that have a bound cyt c_2. From the net change in absorption, ΔA, at both wavelengths, the molar ratio RC/cyt c_2 was calculated using eq 2 (note that the path length, l, cancels out). The experimental values for the absorbance changes shown in Figure 2b are $\Delta A_{502} = 0.0223 \pm 0.0010$ and $\Delta A_{545} = 0.0156 \pm 0.0010$, resulting in a RC/cyt c_2 ratio of 3.9 ± 0.7. Using the values of the amplitudes at $t = 0$ and $t \gg \tau_e$, eq 2 gives a ratio of RC/cyt c_2 of 4.1 ± 0.4 (for $\lambda = 545$ nm) and 3.9 ± 0.6 (for $\tau = 502$ m). The weighted average of the optical measurements is 4.0 ± 0.3. Since both the optical measurements and SDS−PAGE (see above) give, within experimental error, the same RC/cyt c_2 ratios, we conclude that the cyt c_2 in the co-crystal is active in fast electron transfer to D^+.

Proposed Model of the RC−Cyt c_2 Structure. *(A) Determination of the RC Position by Molecular Replacement*. The three-dimensional structures of both the RC and cyt c_2 have been previously determined (Allen *et al*., 1986, 1987a,b, 1988; Yeates *et al*., 1987; Chang *et al*., 1991; El-Kabbani *et al*., 1991; Chirino *et al*., 1994; Ermler *et al*., 1994; Arnoux *et al*., 1995; Axelrod *et al*., 1994); consequently, the molecular replacement technique was used to determine the co-crystal structure. The RC contributes the majority of the scattering material in the co-crystal and was therefore used as the search model for the molecular replacement procedure. Rotation functions were calculated using all measured reflections between 6 and 15 Å resolution. The rotation function (with a 35 Å Patterson integration radius) showed a peak 4σ above the background which was 1.4 times higher than the next highest peak. The position of the rotated RC model in the unit cell (the translation function) was then determined with a modified version of the program RVAMAP from MERLOT (Crowther, 1972) which uses the correlation coefficient to maximize the fit between the observed and calculated structure factors at different translation values along the crystallographic axes (Tim McPhillips, Department of Chemistry, California Institute of Technology, personal comunication). Because of the space group ambiguity, the translation search was carried out for the eight possible primitive space groups of protein crystals that belong to the Laue class *P*4/*mmm*. A translation function peak was found for the space group $P4_32_12$ which was 5 times larger than the next highest peak and 6σ above the background. Peaks of similar amplitude were not found in any of the other possible space groups. Optimization of the RC model position (obtained from the rotation and translation functions) by rigid body refinement (using all reflections to 4.5 Å) led to an R factor of 0.44 ($R = \sum(F_o - F_c)/\sum F_o$), where F_o and F_c are the observed and calculated model structure factors, respectively). The rigid body refined Euler angle rotation function solutions were $\alpha = 54.6°$, $\beta = 61.0°$, and $\gamma = 55.8°$. The translation vector was 0.76, 0.08, 0.36 (fractions of the unit cell dimensions along the x, y, and z axes, respectively). The RC subunits, positioned according to the molecular replacement solution, packed satisfactorily within the tetragonal cell (Figure 3). All lattice contact points were between hydrophilic domains of the RC, and there is no interpenetration of symmetrically related molecules.

FIGURE 3: Part of the crystal unit cell showing packing interactions between symmetry-related RCs. RC subunits: L (yellow), M (blue), and H (green). A symmetry-related RC molecule is shown in black. Patches of electron density ($2F_o - F_c$), 2σ above the background level, are shown in pink above the M subunit on the periplasmic side of the RC. This electron density is attributed to cyt c_2.

The molecular replacement indicated one RC [MW = 101 000 (Williams *et al*., 1986)] or one RC−cyt c_2 molecular complex [MW = 115 000; the molecular weight of cyt c_2 is 14 000, (Bartsch 1978)] in the asymmetric unit and eight molecules in the unit cell. This packing results in a ratio of unit cell volume to protein molecular weight of V_m = 6.2 Å^3/Da at an RC/cyt c_2 ratio of 4. This is larger than that found for most crystals of soluble proteins which have typical ratios of V_m = 2.5−3.5 Å^3/Da (Matthews, 1968). Such a high solvent content as found in the co-crystal (∼74%) has also been found for other membrane protein crystals (Roth *et al*., 1989; Krauss *et al*., 1993; Kerfield *et al*., 1993). Orthorhombic RC crystals (Allen *et al*., 1987) have a smaller ratio of unit cell volume to protein molecular weight (V_m = 3.8 Å^3/Da) than that found for the co-crystals.[4]

(B) Determination of the Cyt c_2 Position. A similar attempt to find a molecular replacement solution for the cyt c_2 molecule was unsuccessful, presumably because of the much lower contribution to the scattering material in the crystal, due to both the low molecular weight of cyt c_2 and the low occupancy. A similar situation was found in the case of the yeast cytochrome *c* peroxidase−iso-1-cytochrome *c* structure (Pelletier & Kraut, 1992).

To try to identify the location of the cyt c_2 molecule, difference electron density maps ($F_o - F_c$ and $2F_o - F_c$) were calculated. The $2F_o - F_c$ map, visualized using the interactive graphics program FRODO (Jones, 1985), showed electron density above the solvent-exposed periplasmic surface of the RC molecule where the cyt c_2 is known to bind in solution (Prince *et al*., 1975; Rosen *et al*., 1983). The map, however, was noisy, and the position of the cyt c_2 could not be determined. To improve the quality of the electron density, the RC model was refined using the geometry restraints in the least squares refinement program TNT (Tronrud *et al*., 1987). Following one cycle of constrained coordinate refinement, the *R* factor within the resolution range of 4.5−25 Å was 0.38. The refined RC structure had a root mean square deviation from ideal bond lengths of 0.03 Å and from ideal bond angle of 3.5 Å.

Following refinement, regions of the difference electron density map were compared to the positions of the RC molecules. An extensive search for difference electron density outside the surface of the RC molecules was performed. Patches of difference electron density (1.5−3σ above the background) continued to be observed on the periplasmic side of the M subunit of an RC molecule and adjacent to part of the cytoplasmic domain of the H subunit of a second, symmetry-related RC molecule (Figure 3). The difference electron density in this area was in discontinuous patches and could not be fitted directly with the structural model of the cyt c_2. No significant difference electron density at this level was detected in other regions on the surface of the RC. We attribute the observed difference electron density to the presence of cyt c_2 at this position in the co-crystal.

(C) Introduction of the Cyt c_2 Structure into the Model. Having been unable to determine the exact position of the cyt c_2 from the electron density map, we positioned it manually into the difference electron density above the M subunit using the following criteria: (i) the cyt c_2 was positioned by overlapping its known structure (Axelrod *et al*., 1994) with the electron density; (ii) the cyt c_2 was oriented such that the terminal methyl group (CBC) in the exposed cleft (Axelrod *et al*., 1994) was toward the RC and the heme was in a patch of electron density; and (iii) there was no interpenetration between the cyt c_2 and the two RC molecules that form lattice contacts (Figure 3). Following this gross positioning, an examination of the $2F_o - F_c$ electron density map in the area of the cyt c_2 showed a number of negatively charged and polar residues on the L and M subunits of the RC, associated with electron density which indicated that they might serve as contact points for lysine residues on the cyt c_2 (Allen *et al*., 1987; Tiede *et al*., 1988; Tiede & Chang, 1988). The cyt c_2 was rotated to bring lysines into close proximity with these RC residues, without grossly altering the position as determined previously. The resulting proposed model of the RC−cyt c_2 complex is shown in Figure 4.

Some of the features of the RC−cyt c_2 complex are the following: The cyt c_2 is in contact with both the L and M subunits of the RC, consistent with cross-linking experiments (Rosen *et al*., 1983). The closest edge to edge distance between the heme and to both D_A and D_B is ∼14 Å; the nearest RC amino acid residue to the heme edge is Asp-M184. The normal to the heme plane intersects the membrane normal at an angle of ∼80°, which is similar to the value of 69.7° obtained from linear dichroism measurements (Tiede, 1987). The angle between the ring planes of D and the heme is ∼20°. Pairs of amino acid residues in close proximity are Gln-L264:Lys-Cyt88, Asp-L257:Lys-Cyt95, Asp-L261:Lys-Cyt97, Gln-L258:Lys-Cyt99, Asp-M88:Lys-Cyt103, and the backbone carboxyl of Gln-M77:Lys-Cyt105. An additional contact is made between cyt c_2 and the H subunit of the RC on the symmetry-related molecule (compare Figure 3 with Figure 4). This additional contact is not found in solution or *in vivo*. It is possible that the position of the cyt c_2 in the crystal lattice has been stabilized by this additional contact.

Additional Crystallographic Analyses. The cyt c_2 orientation in the co-crystal model was performed manually, using the criteria described above. As this procedure may result in inaccuracies, further crystallographic analyses were performed to substantiate the assigned position.

(A) Omit Maps. The reliability of the co-crystal model was assessed by the omit map technique (Bhat & Cohen, 1984). Deletion of 150 residues of the L subunit followed by least squares coordinate refinement resulted in $F_o - F_c$ difference electron density, which closely followed the positions of the deleted peptide chain, supporting the positioning of the RC based on the molecular replacement solution. This method was also used to provide support for the position of the cyt c_2 and assess the possibility of phase bias. The cyt c_2 structure, with the heme deleted, was again entered into the electron density patch above the M subunit, and the resulting model was refined. A calculated $F_o - F_c$ difference electron density map showed positive electron density contoured around the missing heme position (Figure 5). If the cyt c_2 was positioned in alternate positions (such as rotating the cyt c_2 by 180° with respect to the RC or adjacent to the membrane spanning area of the RC), and omit maps were calculated, no significant electron density could be detected (data not shown). These results support the proposed co-crystal model.

[4] In the calculations of these ratios the detergent molecules were not included in the MW of the RC.

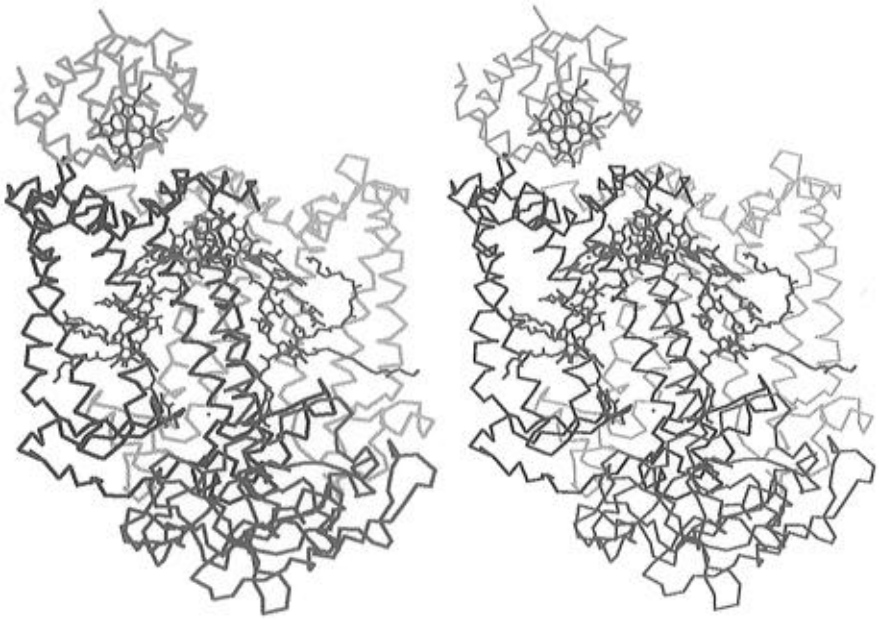

FIGURE 4: Stereoview of the proposed model of the *Rb. sphaeroides* RC−cyt c_2 complex, with the RC subunits, L (yellow), M (blue), and H (green), the cyt c_2 polypeptide (cyan), and the RC cofactors and heme (red).

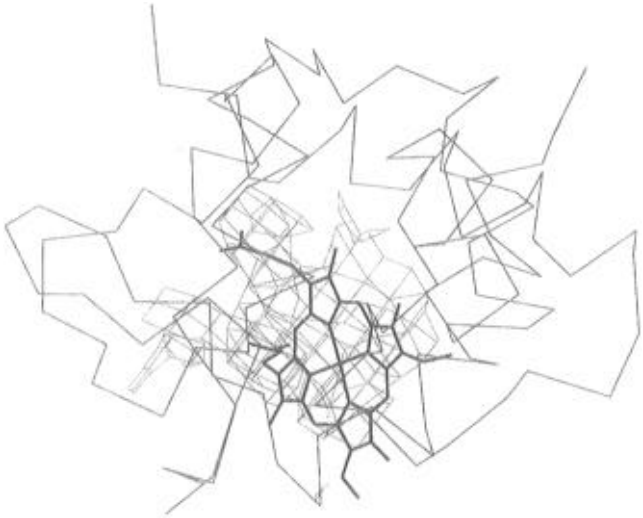

FIGURE 5: Omit map calculated from a model of the RC−cyt c_2 using the known structures of these proteins (Allen *et al*., 1987; Axelrod *et al*., 1994) in the positions proposed in the co-crystal structure. The cyt c_2 heme was deleted, and then eight cycles of least squares coordinate refinements were performed. The presence of $F_o - F_c$ difference electron density (2σ above the background level, shown in pink) roughly follows the contours of a heme (shown in red for clarity). This indicates the presence of a cyt c_2 heme at this position in the co-crystal. The cyt c_2 polypeptide (cyan) is shown for reference.

(B) Additional Refinement. The possibility that the patches of difference electron density near the periplasmic surface of the RC were due to inaccuracies in the RC structure at the early stages of refinement was investigated. If this were the case, further coordinate refinement of the RC structure (without the cyt c_2) should improve the model and result in the elimination of the patches of difference electron density. This refinement was performed to an *R* factor of 0.28. During the refinement process, the match between the difference electron density and the RC model improved, and concomitantly, the difference electron density in most areas not occupied by the RC model diminished. However, the patches of difference electron density near the periplasmic side of the RC, above the M subunit, did not diminish, providing further evidence that this difference electron density is a result of the presence of cyt c_2 bound at this site in the co-crystal.

(C) Analysis of the Effect of Occupancy and Resolution on the Apparent Electron Density of Cyt c_2. The combination of the low occupancy of the cyt c_2 in the co-crystals and the low resolution X-ray diffraction data is the likely reason for the noncontiguous difference electron density above the M subunit. To ascertain whether this was the case, a model of the RC−cyt c_2 complex was built using the known structures of the RC and cyt c_2 (Allen *et al*., 1987; Axelrod *et al*., 1994) in the co-crystal positions. Electron density was calculated directly from this model using TNT (Tronrud *et al*., 1987), by calculating $\sum F_{model} \exp(i\alpha_{model})$, where both the structure factors (F) and phases (α) were obtained solely from the model and the summation was over all atoms. The calculations were performed at different resolutions and cyt c_2 occupancies. In Figure 6, the electron density above the periplasmic side of the M subunit is shown for RC/cyt c_2 ratios of 1 (Figure 6, top) and 3 (Figure 6, bottom), at 4.5 Å resolution. The electron density becomes less contiguous as the occupancy decreases, and at a ratio of 3, the electron density is broken up into patches, similar in appearance to the electron density observed in the co-crystal (see Figure 3). Calculating similar maps at 3 Å resolution had little effect on the appearance of the patches. These calculations indicate that the appearance of the observed electron density patches is primarily the result of the low cyt c_2 occupancy.

Lowest Energy Cyt c_2 Docking Models. The interaction between the RC and cyt c_2 has been shown to be primarily electrostatic (Okamura & Feher, 1983; Long *et al*., 1989; Rongey *et al*., 1994). Therefore, it is likely that the most stable RC−cyt c_2 complex is in a minimum with respect to electrostatic interaction between the proteins. Using the algorithm described in the Experimental Procedures section, $\sim 2 \times 10^7$ possible structures were constructed. The mean electrostatic energy was $\sim +50$ meV with a standard deviation ~ 60 meV. The 1000 lowest structures, as identified by the searching algorithm, had interaction energies that were

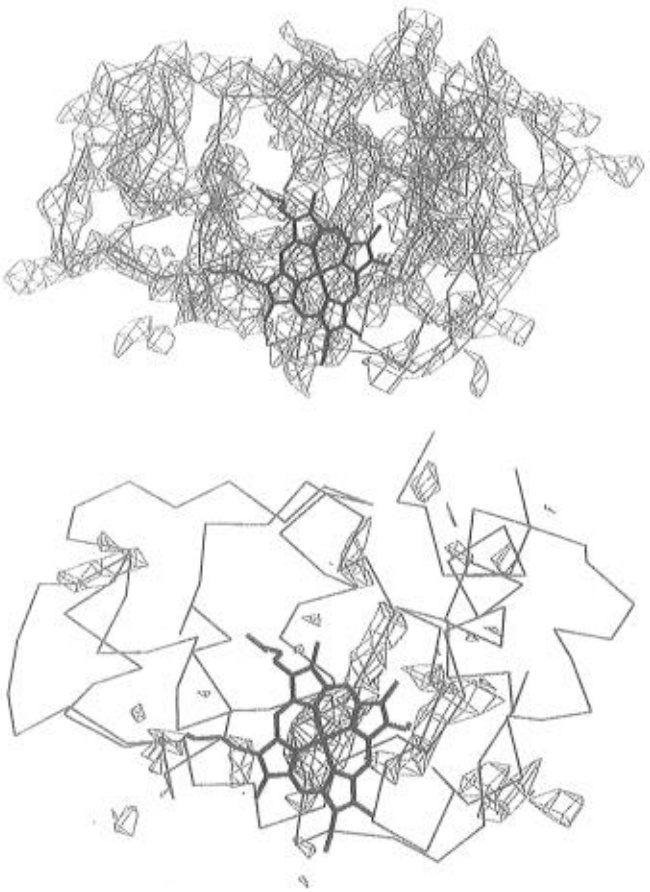

FIGURE 6: Theoretical F_c electron density maps in the region of the cyt c_2, calculated from the known structures of the cyt c_2 (Axelrod *et al*., 1994) and RC (Allen *et al*., 1987) which were superimposed on the co-crystal model for two different RC/cyt c_2 ratios: (top) 1 and (bottom) 3. The cyt c_2 polypeptide (cyan) and heme (red) are shown for clarity. The electron density, in pink (1σ above the background level), was obtained by calculating $\sum F_{model} \exp(i\alpha_{model})$ over all the atoms of the model. Note the discontinuous electron density for an RC/cyt c_2 ratio of 3; this is similar to the results obtained for the electron density map of the co-crystal (see Figure 3).

beyond three standard deviations from the mean energy (i.e., energies lower than −130 meV). The electrostatic interaction energy for each of these 1000 structures was calculated more accurately (see Experimental Procedures), and the structures were compared with the co-crystal model. The docked RC−cyt c_2 complex that was calculated to have the lowest interaction energy is compared to the structure of the co-crystal model in Figure 7 (only the hemes are shown). Two views are shown: in Figure 7a, a side view, similar to that in Figure 4, and in Figure 7b, a view along the 2-fold symmetry axis of the RC facing the periplasmic surface. The lowest energy-docked structure had a −154 meV interaction energy.[5] The next 11 lowest energy structures all had similar orientations and positions. As the energies became less favorable, the relevant structures were found further away from the co-crystal position, but were still on the M subunit side of the RC.

The lowest energy structure (of which the heme is shown in green) has the same orientation as the cytochrome in the co-crystal model. Notice how the propionic acid groups

[5] The calculated interaction energy for the co-crystal structure was −176 meV.

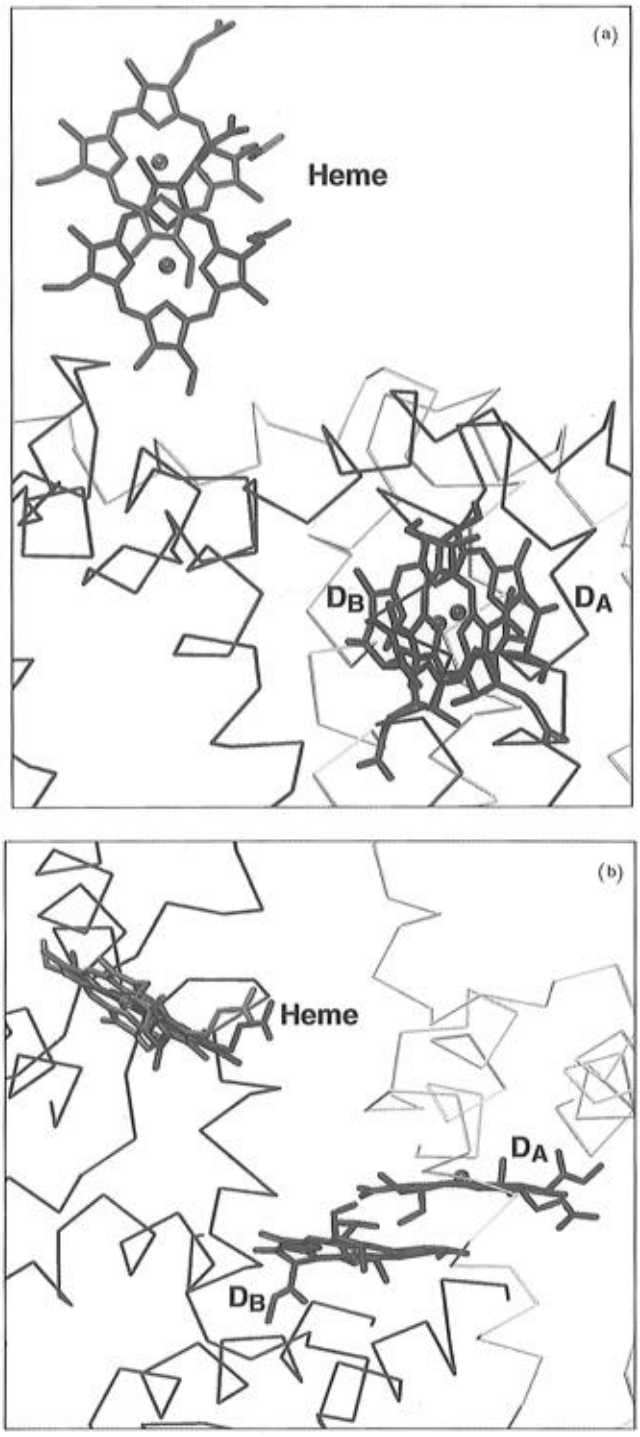

FIGURE 7: Comparison between the heme position of the proposed co-crystal structure (red) and the lowest electrostatic energy structure (green). (a) Side view, looking perpendicular to the membrane normal (similar to that shown in Figure 4). (b) Top view, looking down on the periplasmic surface along the membrane normal. The orientation of the heme is the same for both structures; the displacement of the heme (panel a) is a consequence of the algorithm which assumes rigid bodies (see text). The primary donor D (bacteriochlorophyll dimer, red) is shown for orientation purposes.

(Axelrod *et al*., 1994) of the two hemes are oriented in a similar direction in Figure 7a and how the planes of the two hemes are nearly parallel in Figure 7b.

The search algorithm utilizes the RC and cyt c_2 structures as rigid bodies and thus does not predict docked structures that are as close to the RC as in the co-crystal model (see relative heme positions in Figure 7a). As a result, the heme

Table 2: Electron Transfer and Binding Coefficients between Cyt c_2 and Wild-Type and Mutant RC[a]

strain	τ_e (μs)[b]	k_0 (M^{-1} s^{-1})[b]	K_D (M)[b]
native	0.8 ± 0.1	$(9 \pm 2) \times 10^8$	$(5 \pm 1) \times 10^{-7}$
DK(L155)	0.9 ± 0.1	$(7 \pm 1) \times 10^8$	$(6 \pm 1) \times 10^{-6}$
DK(M184)	0.8 ± 0.2	$(7 \pm 1) \times 10^7$	$(3 \pm 1) \times 10^{-4}$

[a] Experimental conditions: 10 mM HEPES (pH = 7.5), 0.04% (w/v) DM, 0.1 mM Q_0 and Q_0H_2, each, and 0.1 mM EDTA at 23 °C. The RC concentration was 1 or 10 μM, and the cyt c_2 concentration was varied between 0 and 400 μM. The change in absorption due to reduction of D^+ by cyt c_2^{2+} was monitored at 595 or 805 nm. [b] The parameters τ_e (first-order time constant), k_0 (second-order rate constant), and K_D (dissociation constant for the cyt c_2−RC complex) were determined as described in the Experimental Procedures section.

iron for the lowest energy structure is ~5 Å from the iron in the co-crystal model. In addition, these calculations take into account only electrostatic interactions (with the limitations discussed in the Experimental Procedures section). In view of these approximations, we consider the agreement between the lowest energy docked structure and the co-crystal model to be very good.

Electron Transfer and Binding Affinity of Site-Directed Mutants. A method of identifying the area of contact between the RC and the cyt c_2 is to modify the periplasmic surface of the RC and test the effect of the modification on electron transfer and binding affinity of the cyt c_2. We modified the RC surface by selectively mutating specific residues believed to be important in binding. This effectively "maps" the part of the periplasmic surface that interacts with the cyt c_2. Mapping the entire surface will require the engineering of many mutants. The results of the first two mutants are presented here.

Two aspartic acid (Asp) residues, at positions L155 and M184 on the periplasmic surface of the RC, were changed to lysine (Lys) residues. They are located in different regions of the periplasmic surface (Figure 8) and are in symmetry-related positions with respect to the 2-fold symmetry axis of the RC. These residues have previously been proposed to interact with Lys residues of cyt c_2, stabilizing the bound complex (Allen *et al*., 1987; Mathis, 1994; Tiede, 1987; Tiede *et al*., 1988). Modification of a residue that stabilizes the complex is expected to reduce the binding affinity of the cyt c_2 to the RC. To determine the effects of these mutations on RC−cyt c_2 interactions, electron transfer between these proteins was measured and their binding affinities were determined.

An example of these measurements for native and mutant RCs is shown in Figure 9, where the time dependence of the fraction of photooxidized D following a laser flash is plotted. The traces exhibit biphasic kinetics. The fast phase decays with a first-order rate constant and is due to the cyt c_2 bound to the RC prior to the laser flash. The characteristic time of this process (not resolved in Figure 9) is $\tau_e \cong 1$ μs (see Table 2). The slow phase decays with a second-order rate constant, k_0, and is determined by the diffusion of cyt c_2 in an electrostatic field. From the relative amplitudes of the fast and slow phase at different cyt c_2 concentrations, the dissociation constant, K_D, was determined as described in the Experimental Procedures section. The values of τ_e, k_0, and K_D for the native and mutant RCs are summarized in Table 2. The rate of fast electron transfer, τ_e, from cyt c_2 to D^+ was within experimental error, the same for the mutant

FIGURE 8: Distribution of charged residues at the RC−cyt c_2 interface as viewed from the top along the membrane normal (similar to Figure 7b). Basic residues (Arg, Lys) are on the RC (thin blue lines) and the cyt c_2 (thick blue lines). Acidic residues (Asp, Glu) are on the RC (thick red lines) and on the cyt c_2 (thin red lines). The two aspartic acid residues that have been mutated are shown by extra heavy (red) lines. The cyt c_2 heme (magenta) and D (magenta) are shown for reference. The polypeptide chains of the RC subunits L (yellow) and M (blue) have been truncated below D.

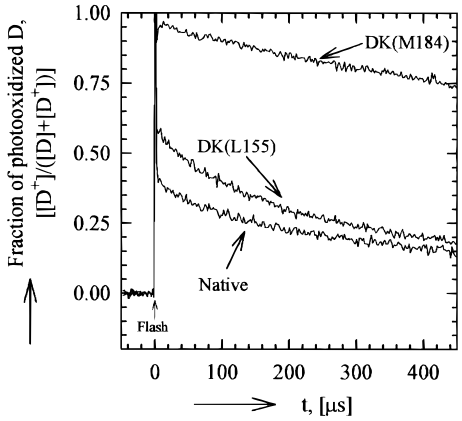

FIGURE 9: Electron transfer kinetics of D^+ reduction by cyt c_2 in native and mutant [DK(M184) and DK(L155)] RCs. The kinetics were monitored by measuring absorption changes at 595 nm as a function of time following flash-induced charge separation. Absorption changes were normalized to the total RC concentration. The kinetics are biphasic. The fast phase ($\tau \sim 1$ μs) is due to cyt c_2 bound to the RCs; the kinetics of this phase were measured separately and are not resolved on this time scale. The slow phase represents reduction of D^+ by a second-order reaction with cyt c_2. From an analysis of such data, at different cyt c_2 concentrations, the fast time constant (τ_e), the second-order rate constant (k_0), and the dissociation constant (K_D) were determined (see Table 2). The DK(M184) mutant RCs show a significant decrease in both the amount of bound cyt c_2 and the second-order rate constant, in accord with the proposed RC−cyt c_2 structure. [Conditions: 10 μM RCs and cyt c_2 in 10 mM HEPES (pH = 7.5), 0.04% DM, 0.1 mM EDTA, 0.1 mM Q_0 and Q_0H_2, each].

and for native RCs, suggesting that the mutations did not affect the position of the docked cyt c_2. The dissociation constant, K_D, increased ~600-fold in the DK(M184) mutant but only approximately 10-fold in the DK(L155) mutant. Similarly, the second-order rate constant was decreased significantly (~10-fold) in the DK(M184) mutant but

Table 3: Comparison of Predicted and Observed Effects of Cyt c_2 Binding to Native and Mutant RCs for Different Docking Models[a]

model	proposed interaction at mutation site		predicted order of effect	observed order of effect
	L155	M184		
Allen *et al*.[b]	salt bridge	possible salt bridge	L155 ≥ M184	
Tiede and Chang[c]	separated charge pair	separated charge pair	L155 ≅ M184	M184 ≫ L155
this study	about 20 Å from cyt c_2	in van der Waals contact with heme	M184 ≫ L155	

[a] Salt bridges are assumed to have the strongest interaction, followed by separated charge pairs or possible salt bridges. [b] Allen *et al*. (1987) classified charge pair interactions as either "salt bridges" for close pairs and possible salt bridges for charged pairs farther apart. [c] Tiede and Chang (1988) classified interactions as salt bridges if separated by 2.6−3.6 Å or as separated charge pairs if greater than 5 Å apart.

remained essentially unchanged in the DK(L155) mutant. The much larger effect of the DK(M184) mutation [compared to the DK(L155) mutant] on the binding of cyt c_2 shows that cyt c_2 binds on the M side of the periplasmic surface of the RC (see Figure 8), in agreement with the proposed co-crystal structure.

SUMMARY AND DISCUSSION

Proposed Structure of the RC−Cyt c_2 Complex. The RC and cyt c_2 from *Rb. sphaeroides* were co-crystallized. The ratio of RC/cyt c_2 in the co-crystals was determined to be 4 (Figures 1 and 2). The position of the RC in the unit cell was obtained by molecular replacement (Figure 3). Additional patches of electron density were observed in the vicinity of the periplasmic side of the M subunit of the RC (Figure 3). We ascribe these patches to the presence of cyt c_2. However, the data were not of high enough quality to unambiguously position the cyt c_2. Consequently, we manually positioned the cyt c_2 into the electron density patches with the exposed heme edge toward D and pairing a number of oppositely charged or polar residues on the RC and cyt c_2. The lack of contiguous electron density is predominantly due to the low cyt c_2 occupancy as shown by model calculations (Figure 6).

Further crystallographic analyses were performed to substantiate the correlation between the electron density patches and the position of the cyt c_2. These included (i) the omit map technique (Bhat & Cohen 1984), in which the heme of the cyt c_2 was deleted and omit maps were calculated for different positions of the cyt c_2, and (ii) further refinement of the RC−cyt c_2 structure resulting in a decrease in the background electron density in areas not occupied by the RC without a concomitant decrease in the electron density of the patches assigned to cyt c_2.

Two additional pieces of evidence were presented to corroborate the proposed RC−cyt c_2 structure: (i) The electrostatic interaction energy between the RC and cyt c_2 was calculated for a large number ($\sim 2 \times 10^7$) of structures. The lowest energy structure corresponded closely to the proposed RC−cyt c_2 structure (Figure 7). (ii) Two aspartic acid residues (M184 and L155) were mutated to lysines, and the dissociation constants and electron transfer characteristics were measured (Table 2). The DK(M184) mutation had a much larger effect than the DK(L155) mutation, in accord with the prediction based on the proposed structure of the RC−cyt c_2 complex (compare Figures 7b and 8).

Having shown that the proposed structure of the complex is basically correct, we need to address the question whether the structure in the co-crystal is the same as that in solution. Although this is a general problem that crystallographers face, it is more acute for a macromolecular complex where the binding forces between the molecules of the complex compete with forces imposed by the crystal structure. The mutagenesis work described in this work provides evidence of a semiquantitative nature that the two structures are the same. A more critical test is the electron transfer kinetics between reduced cyt c_2 and the photooxidized primary donor, D^+. This rate is expected to be very sensitive to the position of the cyt c_2 in the structure (Moser *et al*., 1992; Beratan *et al*., 1991). We measured the kinetics in the co-crystal (Figure 2) and found it to be the same as measured in solution (Table 2, native RCs). This result provides strong evidence for the similarities between the structures in the co-crystal and in solution.

Comparison between Different Proposed RC−Cyt c_2 Models. *(A) The Cyt c_2 Binding Site*. As described in the introduction, two models for the RC−cyt c_2 complex have been described previously (Allen *et al*., 1987; Tiede & Chang, 1988). In Table 3 we compare the predicted results for the DK(M184) and DK(L155) mutants on the cyt c_2 binding for the proposed structures. In the structure proposed in this work, residue M184 is in contact with cyt c_2; we consequently expect that changing this residue would have a large effect on cyt c_2 binding. Changing residue L155 should have a smaller effect because of its larger distance from the cyt c_2. As shown in Table 3, the observed effects of these two mutations on cyt c_2 binding are in agreement with these predictions.

In the model proposed by Allen *et al*. (1987), obtained by manual docking, cyt c_2 forms four definite salt bridges and five possible salt bridges. The cyt c_2 position in this model is directly above D, similar to that of the cyt *c* in RCs from *Rp. viridis*. For their model, we predict that modification of L155 should have a larger or equal effect on cyt c_2 binding than modification of M184. This prediction is in disagreement with the observed results (see Table 3).

In the model proposed by Tiede and Chang (1988), the cyt c_2 is shifted toward the M side of the RC, although not as much as in our model. In their study, the cyt c_2 was first docked manually using a graphic display and then rotated around a defined axis, using energy minimization calculations to find possible docking sites. This search identified a site with six possible salt bridges and five separated charge pairs between the RC and cyt c_2. For their model, we predict that changing residues L155 or M184 should have comparable effects on cyt c_2 binding, which is in disagreement with our observations (see Table 3). Thus, we conclude that the two previously proposed models do not represent the correct RC−cyt c_2 structure.

(B) Interactions between the RC and Cyt c_2. In the co-crystal model presented in this work, we assume a unique binding site. This is in contrast to the conclusion of Tiede *et al*. (1993), who postulate nonspecific binding that arises from a juxtaposition of regions of delocalized complementary

potentials on the RC and cyt c_2. The ability to form RC−cyt c_2 co-crystals favors a unique structure with a well-defined cyt c_2 binding site. Additional support for a specific binding site between electron transfer proteins is provided by work on two other complexes: the yeast cytochrome *c* peroxidase−iso-1-cytochrome *c* complex (Pelletier & Kraut, 1992) and the mitochondrial ferredoxin−cytochrome P450 complex (Coghlan & Vickery, 1992).

Significance of the Proposed RC−Cyt c_2 Structure on Intermolecular Electron Transfer. Two models have been proposed to predict rates of intermolecular electron transfer. Moser *et al*. (1992) proposed a correlation, based on classical Marcus theory (Marcus, 1956), between the electron transfer rate and the donor−acceptor distance, with the intervening protein serving as a uniform medium. Onuchic and Beratan (Beratan *et al*., 1991) proposed the existence of electron transfer pathways whose effectiveness in electron transport depends on both the number of bonds between atoms and the electronic coupling between donor and acceptor prosthetic groups.

In the proposed co-crystal model, the heme is ∼14 Å from the special bacteriochlorophyll pair D of the RC (edge to edge). This distance is reasonable for an electron transfer rate of ∼1 μs according to Moser *et al*. (1992). However, a specific electron transfer path may exist. The closest RC amino acid to the heme is Asp-M184, which is in van der Waals contact with a terminal heme methyl group. Following the polypeptide chain from M184 is Trp-M185 and Thr-M186. Thr-M186 is in van der Waals contact with the B half of the bacteriochlorophyll dimer D [e.g., Feher *et al*. (1989)]. Recently, Aquino *et al*. (1995) used the Onuchic and Beratan model to predict likely pathways for electron transfer from cytochromes to D^+ for both *Rps*. *viridis* and *Rb*. *sphaeroides*. In that study, Asp-M184 was shown to be strongly coupled electronically to D. Thus, M184, M185, and M186 provide a likely electron transfer path to D_B.

In the measurements performed on the DK(M184) RC mutant, it is surprising that while the replacement of aspartic acid with lysine perturbs the binding of the cyt c_2, the rate of electron transfer from bound cyt c_2 is not altered. One might expect a change in the effectiveness of the electron pathway as well as a change in the driving force brought about by the change in charge of the mutated M184 residue (Ortega & Mathis, 1993; Lin *et al*., 1994). A possible explanation of the unchanged kinetics is that the two effects compensate for each other. Alternatively, it is possible that lysine and aspartic acid serve as equally efficient members of the electron pathway and that the driving force is unaffected. The latter would occur if the dielectrically weighted distance from the charged M184 residue to the cyt c_2 heme iron is the same as to D^+.

Future Objectives. The main goal is to improve the crystallographic data to allow an unambiguous positioning of the cyt c_2. This will require a higher occupancy of cyt c_2 in the co-crystal, improved resolution of the X-ray diffraction data, and preferably larger crystals. We are currently exploring different crystallization conditions to achieve these goals. One problem is that cyt c_2 precipitates at a lower PEG concentration than RCs (Allen *et al*., 1986). Thus, as crystals grow, the cyt c_2 concentration in the solution drops, causing the incorporation of cytochrome-less RCs in the co-crystal lattice. This is likely to result in incorporation of errors into the lattice which may limit the crystal size (Kam *et al*., 1978; Durbin & Feher, 1990) and order. A different precipitating agent might eliminate this problem.

Other approaches to increase the cytochrome occupancy include chemical cross-linking of cyt c_2 to the RC (Rosen *et al*., 1983) and/or use of site-directed mutagenesis to change neutral residues on the periplasmic side of the RC that face lysines on the cyt c_2 to negatively charged residues (e.g., Gln L264 → Glu or Gln L258 → Glu). The charged Glu−Lys pairs are expected to increase the binding affinity of cyt c_2 to the RC.

More sophisticated computational methods may reveal more about the nature of RC−cyt c_2 docking. Other factors, such as van der Waals interactions and entropy, need to be considered in the energetics of docked configurations. In addition, more sophisticated continuum models (Gilson & Honig, 1988) should be explored in the computation of electrostatic energy, although such models may be too time consuming to apply to the number of structures considered here. Perhaps most important would be the inclusion of side-chain orientation when generating a putative docked structure. The distance between the cyt c_2 and RC in the computer-generated structures was consistently farther than that found in the co-crystal model, even when the heme orientation was similar. It is likely that allowing side-chain reorientation would permit a more tightly bound complex.

The mutagenesis work needs to be extended to map in more detail points of contact between the cyt c_2 and the RC. From the intermolecular electron transfer kinetics in the mutants, the existence of electron transfer pathways (after taking into account steric effects and changes in the driving force) should be identifiable.

ACKNOWLEDGMENT

We thank Doug Rees and his co-workers Barbara Hsu, Mike Stowell, Tim McPhillips, and Kyong-Hee Kim for help with the crystallographic analysis and for helpful discussions, Ed Abresch for help in isolation of the RCs, Andrea Juth for technical assistance with mutagenesis, Tom Macke for help with Figure 7, and Victoria Roberts for helpful discussions.

REFERENCES

Adir, N., Okamura, M. Y., & Feher, G. (1994) *J. Biophys. 66*, A127.
Allen, J. P., & Feher, G. (1984) *Proc. Natl. Acad. Sci. U.S.A. 81*, 4795−4799.
Allen, J. P., Feher, G., Yeates, T. O., Rees, D. C., Deisenhofer, J., Michel, H., & Huber, R. (1986) *Proc. Natl. Acad. Sci. U.S.A. 83*, 8589−8593.
Allen, J. P., Feher, G., Yeates, T. O., Komiya, H., & Rees, D. C. (1987a) *Proc. Natl. Acad. Sci. U.S.A. 84*, 5730−5734.
Allen, J. P., Feher, G., Yeates, T. O., Komiya, H., & Rees, D. C. (1987b) *Proc. Natl. Acad. Sci. U.S.A. 84*, 6162−6166.
Allen, J. P., Feher, G., Yeates, T. O., Komiya, H., & Rees, D. C. (1988) *Proc. Natl. Acad. Sci. U.S.A. 85*, 8487−8491.
Aquino, A. J. A., Beroza, P., Beratan, D. N., & Onuchic, J. N. (1995) *J. Chem. Phys. 197*, 277−288.
Arnoux, B., Gaucher, J. F., Ducruix, A., & Reiss-Husson, F. (1995) *Acta Crystallogr. D51*, 368−379.
Axelrod, H. L., Feher, G., Allen, J. P., Chirino, A., Day, M., Hsu, B. T., & Rees, D. C. (1994) *Acta Crystallogr. D50*, 596−602.
Bartsch, R. G. (1978) in *The Photosynthetic Bacteria* (Clayton, R. K., & Sistrom, W. R., Eds.) pp 249−279, Plenum Press, New York.
Beratan, D. N., Betts, J. N., & Onuchic, J. N. (1991) *Science 252*, 1285−1288.

Bhat, T. N., & Cohen, G. H. (1984) *J. Appl. Crystallogr. 17*, 244−248.
Breton, J., & Vermeglio, A., Eds. (1992) *The Photosynthetic Reaction Center II*, Plenum Press, New York.
Chang, C.-H., Tiede, D., Tang, J., Smith, U., Norris, J., & Schiffer, M., (1986) *FEBS Lett. 205*, 82−86.
Chang, C.-H., El-Kabbani, O., Tiede, D. M., Norris, J., & Schiffer, M. (1991) *Biochemistry 30*, 5352−5360.
Chen, L., Mathews, F. S., Davidson, V. L., Tegoni, M., Rivetti, C., & Rossi, G. L. (1993) *Protein Sci. 2*, 147−154.
Chirino, A. J., Lous, E. J., Huber, M., Allen, J. P., Schenk, C. C., Paddock, M. L., Feher, G., & Rees, D. C. (1994) *Biochemistry 33*, 4584−4593.
Coghlan, V. M., & Vickery, L. E. (1992) *J. Biol. Chem. 267*, 8932−8935.
Crowther, R. A. (1972) in *The Molecular Replacement Method* (Rossmann, M. G., Ed.) pp 173−178, Gordon Breach, New York.
Deisenhofer, J., & Michel, H. (1991) *Annu. Rev. Cell Biol. 7*, 1−23.
Deisenhofer, J., Epp, O., Miki, K., Huber, R., & Michel, H. (1984) *J. Mol. Biol. 180*, 385−398.
Deisenhofer, J., Epp, O., Miki, K., Huber, R., & Michel, H. (1985) *Nature 318*, 618−624.
Durbin, S. D., & Feher, G. (1990) *J. Mol. Biol. 212*, 763−774.
El-Kabbani, O., Chang, C.-H., Tiede, D. M., Norris, J., & Schiffer, M. (1991) *Biochemistry 30*, 5361−5369.
Ermler, U., Fritzsch, G., Buchanan, S. K., & Michel, H. (1994) *Structure 2*, 925−936.
Feher, G. (1992) *J. Chem. Soc., Perkin Trans. 2*, 1861−1874.
Feher, G., & Okamura, M. Y. (1978) in *The Photosynthetic Bacteria* (Clayton, R. K., & Sistrom, W. R., Eds.) pp 349−386, Plenum Press, New York.
Feher, G., Allen, J. P., Okamura, M. Y., & Rees, D. C. (1989) *Nature 339*, 111−116.
Fitzgerald, P. M. D. (1988) *J. Appl. Crystallogr. 21*, 273−278.
Gilson, M. K., & Honig, B. (1988) *Proteins 4*, 7−18.
Gunner, M. R. (1991) in *Current Topics in Bioenergetics* (Lee, C. P., Ed.) Vol. 16, pp 319−367, Academic Press, New York.
Hagler, A. T., Huler, E., & Lifson, S. (1974) *J. Am. Chem. Soc. 96*, 5319−5327.
Jones, T. A. (1985) *Methods Enzymol. 115*, 157−171.
Kam, Z., Shore, H. B., & Feher, G. (1978) *J. Mol. Biol. 123*, 539−555.
Kerfeld, C. A., Thornber, J. P., & Yeates, T. O. (1993) *Protein Sci. 2*, 1352−1355.
Kleinfeld, D., Okamura, M. Y., & Feher, G. (1984) *Biochim. Biophys. Acta 766*, 126−140.
Krauss, N., Hinrichs, W., Witt, I., Fromme, P., Pritzkow, W., Dauter, Z., Betzel, C., Wilson, K. S., Witt, H. T., & Saenger, W. (1993) *Nature 361*, 326−331.
Laemmli, U. K. (1970) *Nature 227*, 680−685.
Lendzian, F., Huber, M., Isaacson, R. A., Endeward, B., Plato, M., Bonigk, B., Mobius, K., Lubitz, W., & Feher, G. (1993) *Biochim. Biophys. Acta 1183*, 139−160.
Lin, X., Williams, J. C., Allen, J. P., & Mathis, P. (1994) *Biochemistry 33*, 13517−13523.
Long, J. E., Durham, B., Okamura, M. Y., & Millett, F. (1989) *Biochemistry 28*, 6970−6974.
Marcus, R. A. (1956) *J. Chem. Phys. 24*, 966−978.
Mathis, P. (1994) *Biochim. Biophys. Acta 1187*, 177−180.
Matthews, B. W. (1968) *J. Mol. Biol. 33*, 491−497.
McPherson, A. (1990) *Eur. J. Biochem. 189*, 1−23.
Michel, H., & Deisenhofer, J. (1988) *Biochemistry 27*, 1−7.
Moore, G. R., & Pettigrew, G. W. (1990) *Cytochromes c: Evolutionary, Structural and Physiochemical Aspects*, Springer Series in Molecular Biology, Springer-Verlag, Berlin.
Moser, C. C., & Dutton, P. L. (1988) *Biochemistry 27*, 2450−2461.
Moser, C. C., Keske, J. M., Warncke, K., Farid, R. S., & Dutton, P. L. (1992) *Nature 355*, 796−802.
Okamura, M. Y., & Feher, G. (1983) *Biophys. J. 41*, 122a.
Ortega, J. M., & Mathis, P. (1993) *Biochemistry 32*, 1141−1151.
Overfield, R. E., Wraight, C. A., & Devault, D. (1979) *FEBS Lett. 105*, 137−142.
Paddock, M. L., Rongey, S. H., Feher, G., & Okamura, M. Y. (1989) *Proc. Natl. Acad. Sci. U.S.A. 86*, 6602−6606.
Paddock, M. L., McPherson, P. H., Feher, G., & Okamura, M. Y. (1990) *Proc. Natl. Acad. Sci. U.S.A. 87*, 6803−6807.
Pelletier, H., & Kraut, J. (1992) *Science 258*, 1748−1755.
Prince, R. C., Baccarini-Melandri, A., Hauska, G. A., Melandri, B. A., & Crofts, A. R. (1975) *Biochim. Biophys. Acta 387*, 212−227.
Rees, D. C., Komiya, H., Yeates, T. O., Allen, J. P., & Feher, G. (1989) *Annu. Rev. Biochem. 58*, 607−633.
Roberts, V. A., Freeman, H. C., Olson, A. J., Tainer, J. A., & Getzoff, E. D. (1991) *J. Biol. Chem. 266*, 13431−13441.
Rongey, S. H. (1994) Ph.D. Thesis, University of California, San Diego.
Rongey, S. H., Juth, A. L., Feher, G., & Okamura, M. Y. (1994) *Biophys. J. 66*, A228.
Rosen, D., Okamura, M. Y., & Feher, G. (1980) *Biochemistry 19*, 5687−5692.
Rosen, D., Okamura, M. Y., Abresch, E. C., Valkirs, G., & Feher, G. (1983) *Biochemistry 22*, 335−341.
Rossman, M. G. (1990) *Acta Crystallogr. 46*, 73−82.
Roth, M., Lewit-Bentley, A., Michel, H., Deisenhofer, J., Huber, R., & Oesterhelt, D. (1989) *Nature 340*, 659−662.
Tiede, D. M. (1987) *Biochemistry 26*, 397−410.
Tiede, D. M., & Chang, C.-H. (1988) *Isr. J. Chem. 28*, 183−191.
Tiede, D. M., Budil, D. E., Tang, J., El-Kabbani, O., Norris, J. R., Chang, C.-H., & Schiffer, M. (1988) in *The Photosynthetic Bacterial Reaction Center: Structure and Dynamics* (Breton, J., & Vermeglio, A., Eds.) NATO ASI Series A: Life Sciences, Vol. 149, pp 13−20, Plenum Press, New York.
Tiede, D. M., Vashishta, A.-C., & Gunner, M. R. (1993) *Biochemistry 32*, 4515−4531.
Tronrud, D. E., Ten Eyck, L., & Matthews, B. W. (1987) *Acta Crystallogr. A43*, 489−501.
Wachtveitl, J., Farchaus, J. W., Mathis, P., & Oesterhelt, D. (1993) *Biochemistry 32*, 10894−10904.
Williams, J. C., Steiner, L. A., & Feher, G. (1986) *Proteins 1*, 312−325.
Yang, A.-S., Gunner, M. R., Sampogna, R., Sharp, K., & Honig, B. (1993) *Proteins 15*, 252−265.
Yeates, T. O., Komiya, H., Rees, D. C., Allen, J. P., & Feher, G. (1987) *Proc. Natl. Acad. Sci. U.S.A. 84*, 6438−6442.

BI9522054